Fine-Grained Respiration Monitoring During Overnight Sleep Using IR-UWB Radar

Siheng Li[1,2], Zhi Wang[1,2], Fusang Zhang[1,2,3], and Beihong Jin[1,2(✉)]

[1] State Key Laboratory of Computer Science, Institute of Software, Chinese Academy of Sciences, Beijing 100190, China
{lisiheng19,wangzhi20,zhangfusang,jbh}@otcaix.iscas.ac.cn
[2] University of Chinese Academy of Sciences, Beijing 100190, China
[3] State Key Laboratory for Novel Software Technology, Nanjing University, Nanjing 210093, China

Abstract. Recently, vital sign and sleep monitoring using wireless signals has made great progress. However, overnight respiration monitoring remains a challenge due to human unconscious and uncontrollable movements during sleep. In the paper, we explore the potential of an IR-UWB radar and implement a fine-grained overnight respiration monitoring prototype. Particularly, we exploit the complementarity between amplitude and phase of the radar signal to eliminate blind spots, thus improving the detection rate of overnight respiration monitoring. Moreover, we propose a circle fitting based phase restoration algorithm to correct the respiration depth distortion, and further recognize four respiration patterns (i.e., apnea pattern, Tachypnea pattern, Kussmaul pattern and rapid change pattern of respiration rate), thus enabling fine-grained respiration monitoring during overnight sleep. The experimental results show that our prototype achieves high respiration detection rates and accurate respiration rates, outperforming the two existing approaches. In addition, our prototype has captured the apnea pattern many times in the real sleep scenarios.

Keywords: Contactless sensing · Vital sign monitoring · IR-UWB Radar

1 Introduction

Respiration during sleep is an important indicator of human health, which can reflect the progression of some diseases and decline in health. At the very least, respiration disorders during sleep affect the quality of sleep and cause fatigue during the day. Furthermore, chronic lack of high-quality sleep might lead to obesity [15]. What is worse, severe sleep disorders such as Sleep Apnea Syndrome (SAS) [5] can increase the risk of sudden death in adults. Therefore, it is

T. Hara and H. Yamaguchi (Eds.): MobiQuitous 2021, LNICST 419, pp. 84–101, 2022.
https://doi.org/10.1007/978-3-030-94822-1_5

important to monitor human respiration throughout the night, which is beneficial for diagnosis and treatment of sleep disorders.

In clinical settings, traditional methods for continuous respiration monitoring are capnography [4] and thoracic impedance pneumography [11]. These methods are intrusive and require the subject to stay in hospital or sleep laboratory for a long period of time, which prevents them from wide deployment and in-home use.

Recently, wearable devices such as Flow chest straps [1] have been developed to detect the respiration state but they make users feel uncomfortable while wearing them overnight. The alternative solution is the contactless sensing [2, 18, 19], which is non-intrusive and easy to deploy at home. However, the existing work on respiration monitoring often requires the subject to sit in chair or lie in bed still, limiting the changes in distance and orientation between the subject and the device. Such settings do not match reality. In real scenarios, the subject is completely unconscious and uncontrollable during sleep. Movements of different body parts will cause changes in distance and orientation between the subject and the device. Therefore, overnight respiration monitoring is still a challenge.

In the paper, for overnight respiration monitoring, we explore the ability of the Impulse-Radio Ultra-Wideband (IR-UWB) radar. However, the results of preliminary respiration monitoring experiments are not good enough. We find that, when signal amplitude or phase is used individually for overnight respiration sensing, there exists different blind spots (namely locations where respiration detection experiences poor performance) which are observed for the first time in radar sensing but has been observed in Wi-Fi sensing [22], making it hard to achieve full-time respiration monitoring. Additionally, the human respiration depth estimated from the radar signals has a wide range of variation or even becomes invalid values, which we define as the respiration depth distortion.

We carefully examine the blind spots and the respiration depth distortion, and then offer the solutions and implement a fine-grained overnight respiration monitoring prototype. The main contributions of the paper are as follows.

- We exploit the complementarity between amplitude and phase of received radar signal to eliminate the blind spots and enhance the detectable rate of respiration during overnight sleep, thus enabling overnight respiration monitoring.
- We propose a circle fitting based phase restoration algorithm to restore the signal phase and estimate the real respiration depth, thus solving the respiration depth distortion.
- We combine the respiration rate and respiration depth to identify four respiration patterns that may occur during sleep, including apnea pattern, Tachypnea pattern, Kussmaul pattern and rapid change pattern of respiration rate, thus enabling fine-grained respiration monitoring.
- We conduct extensive experiments to evaluate the performance of our prototype under realistic settings. The experimental results show that our prototype outperforms the two existing approaches and achieves a median error in respiration rate estimation of 0.27 bpm and 100% recognition accuracy for four respiration patterns during sleep.

2 Preliminary Study: Analyzing IR-UWB Signals for Sensing Respiration

As we know, an IR-UWB radar continuously transmits the pulse signals at a certain interval (i.e., Pulse Repetition Interval, PRI) and collects the signals reflected by subjects in the environment. The received signals are down-converted to obtain the I and Q baseband signals, which are recorded in a 2D complex matrix (as shown in Fig. 1), where the row is defined as the "fast time" dimension and the column is defined as the "slow time" dimension. Fast time dimension contains reflective pulse responses with different time delays during a PRI, denoting different distance bins, and slow time dimension updates every PRI [24]. Therefore, when a subject is stationary at a certain position, we can find the fast time bin corresponding to the subject and take a slice along the slow time dimension from the 2D matrix of received signals, getting a 1D time series which is an estimation of the signal reflecting the tiny changes in distance between the subject and the device over time. Visualizing the 1D slice in the IQ domain, we can obtain a series of scattered signal samples, which form an arc-shaped trajectory centered at a certain point. For each signal sample $\boldsymbol{H}$, its amplitude (i.e., $|\boldsymbol{H}|$, denoted by A) and phase (i.e., the angle between $\boldsymbol{H}$ and the I-axis, denoted by θ) can be obtained, the corresponding waveforms are shown in Fig. 2.

In principle, when a subject breathes at rest, the periodic changes in the distance between the subject's chest and the radar will result in the periodic changes in amplitude and phase of the received signal. In other words, the amplitude or phase waveform of the received signal corresponds to the subject's respiration waveform. However, is the principle described above always true? In real sleep scenarios, a subject will move and change his/her sleeping posture and position, which is recorded in the reflected signal. Then, what is the motion-sleep ratio and how does the motion affect the overnight respiration sensing? On the other hand, when a subject faces the radar and breathes, the amplitude increase and decrease of the received signal correspond to the inhalation and exhalation of the body part (e.g., chest), which can reflect the respiration depth theoretically. However, affected by the environment, the magnitude of the signals attenuates nonlinearly as propagating. Therefore, the amplitude difference can only roughly reflect the respiration depth, not precisely correspond to the respiration depth. Different from amplitude, the phase of the received signals is not affected by the environment, and only related to the distance between the human and the radar. That is to say, we can estimate the respiration depth by $\Delta d = -\frac{\lambda}{4\pi}\Delta\Phi$ [3], where λ is the wavelength of the signals, Δd is the change in distance between the human body and the radar over a period of time, and $\Delta\Phi$ is the phase change in the same period of time. However, is this respiration depth estimation method feasible in real sleep scenarios?

We collect the signals of a COTS IR-UWB radar in a real sleep scenario (3 nights of 3 subjects), and analyze the amplitude and phase waveforms of the signals, respectively. The observations we get are as follows.

Observation 1: Respiration is not detectable in all the locations when amplitude or phase of the received signals is used individually.

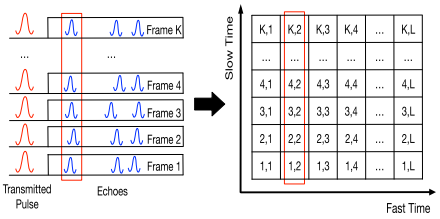

Fig. 1. Received signal matrix.

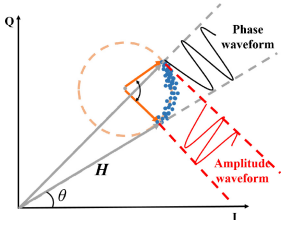

Fig. 2. Signal change patterns of amplitude and phase.

In contrast with the ground truth, we find that about 78% of the amplitude waveforms of the received signals are relatively regular, corresponding to states when the subjects breathe steadily. These waveforms can be regarded as respiration waveforms. Meanwhile, about 10% of the amplitude waveforms correspond to the movements of the subjects which result in more significant changes in the waveform than normal respiration. The amplitude waveforms left are disordered. A similar phenomenon is also observed from the phase waveforms of the signals.

Particularly, we observe that the waveforms differ in different locations and orientations between the subject and the radar. Two examples are shown in Fig. 3. (i) When the subject is lying on the back with his/her sideways chest facing the radar 0.72 m away, the amplitude waveform is disordered while the phase waveform is regular, as shown in Fig. 3(a). (ii) When the subject is lying on one side with his/her chest facing the radar 0.62 m away, the amplitude waveform is regular while the phase waveform is disordered, as shown in Fig. 3(b).

The above results illustrate three points. (i) When a subject breathes normally, whether the amplitude or phase waveform can reflect his/her respiration waveform depends on the distance and orientation between the subject and the radar. (ii) When amplitude or phase of the received signal is used individually, there are locations where the waveforms are disordered and respiration cannot be detected there. We call it the blind spot problem. (iii) The amplitude and phase of the received signal may be complementary to each other, i.e., their blind spots may not overlap. This observation can be used to improve the detection rate of respiration.

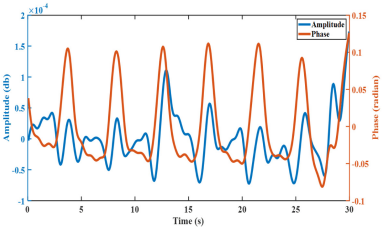

(a) Posture: lying on the back, distance from device: 0.72m.

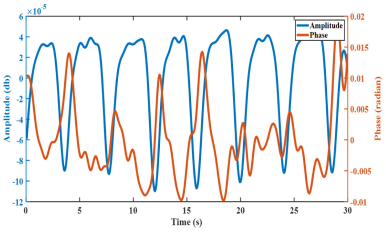

(b) Posture: lying on one side, distance from device: 0.62m.

Fig. 3. Amplitude and phase of two 30 s windows (from a certain subject).

Observation 2: Distortion exists in estimated respiration depth during overnight sleep.

We choose the phase waveform when the subject breathes steadily, calculate the phase changes between all neighboring pairs of peak and valley, and then estimate the respiration depth by $\Delta d = -\frac{\lambda}{4\pi}\Delta\Phi$. We find that the estimated respiration depth has the minimum of 0.01 cm and the maximum of 0.70 cm. However, the depth of 0.01 cm is not a valid respiration depth according to our common sense. By analyzing the estimated method, we know that the distortion of the estimated respiration depth is derived from the distortion of the phase change. That is, the received signals are affected by the multipath phenomenon in the environment. The distance and orientation between a subject and a radar vary during the night, so does his/her sleeping posture. Therefore, the phase we calculate is in fact one distorted by the superposition of these factors. We should eliminate effects of these factors to get more realistic respiration depths.

3 Our Respiration Monitoring Prototype

3.1 Overview

Our respiration monitoring prototype, as shown in Fig. 4, consists of five modules: Signal Preprocessing, Signal Waveform Classification, Respiration Rate Measurement, Respiration Depth Estimation and Respiration Pattern Recognition.

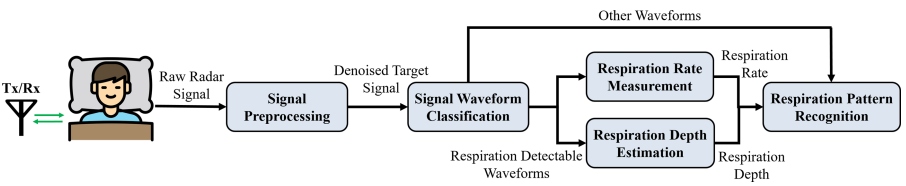

Fig. 4. System architecture of our prototype.

Signal Preprocessing. Signal preprocessing is divided into three steps: background subtraction, human identification and noise reduction. (i) We adopt a 30 s sliding window with none overlay to segment the received radar signals. Then, we apply the background subtraction method in [21] to remove clutter from the original received signals, which is caused by all static reflectors in the background environment, and retain the reflected signal from human body. (ii) Human identification is to identify the signal from human body from the received signal matrix. Here, we use amplitude of the signal for human identification. In detail, given each background-subtracted signal matrix over the 30 s sliding window, we perform FFT along the slow time dimension to obtain a Doppler map. As we know, when the amplitude peak of a column on the Doppler map is within a frequency range of 0.1 Hz to 0.85 Hz, the fast-time index of the largest amplitude peak among all the columns corresponds to the location of

human. Therefore, we take a slice from the 2D original received signal matrix by the fast-time index, and get a 1D time series as an estimation of reflected signal from human body. (iii) We employ the Savitzky-Golay polynomial least squares filter (SG Filter) [10] to remove the high-frequency noise from the signal while preserving the steep changes and remaining the positions of the peaks and valleys [8]. Finally, we perform a detrend operation on the denoised signal to remove the polynomial trend of the time series.

Signal Waveform Classification. After obtaining the reflected signal from human body, we can get the amplitude and phase waveforms of the reflected signal. Then we divide the signal waveforms into three categories: body movement waveforms, respiration detectable waveforms and other waveforms.

We propose a window depth-based method to detect whether the waveform corresponds to a body motion. Specifically, we calculate the phase difference between the maximum and minimum phase values within each 30 s window, and then calculate the relative displacement of human body during each 30 s window, referred to as the window depth. Considering that the window depth is close to the human respiration depth in terms of physical meaning, we set the threshold of window depth to the maximum normal human respiration depth (i.e., 1 cm). If the window depth exceeds this threshold, then we believe a body movement occurs in the current window.

Subsequently, for all the windows without body movements, we apply autocorrelation [23] on both amplitude waveforms and phase waveforms to identify respiration detectable waveforms. The details are described in Sect. 3.2.

After eliminating body movement waveforms and respiration detectable waveforms, the remaining waveforms are referred to as other waveforms, which are generally disordered. However, they might reflect some abnormal information of the human body, so we send them to the Respiration Pattern Recognition module for further processing.

Respiration Rate Measurement. We utilize autocorrelation to measure the respiration rates given respiration detectable waveforms. Figure 5 shows a respiration waveform and its autocorrelation result. We get the lag (shift) of the maximum peak (i.e., N in Fig. 5), and then measure the respiration rate by $\frac{60}{N/f_s}$, where f_s is the radar sampling frequency.

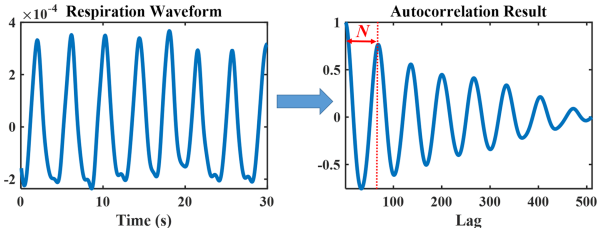

Fig. 5. Applying autocorrelation on respiration waveform.

Respiration Depth Estimation. We estimate the respiration depth given the respiration detectable waveform. We propose a circle fitting based phase restoration algorithm to restore signal phase and estimate the real respiration depth of human, thus solving the respiration depth distortion problem described in Sect. 2. The details of respiration depth estimation are described in Sect. 3.3.

Respiration Pattern Recognition. We combine the respiration rate and respiration depth to recognize four respiration patterns during sleep. The details are in Sect. 3.4.

3.2 Identifying Respiration Detectable Waveform

We identify respiration detectable waveforms by applying autocorrelation on signal waveforms. The autocorrelation function describes the similarity of a signal to a shifted version of itself, and the maximum peak value in the autocorrelation result represents the periodicity of the signal. That is, if the peak value exceeds a certain threshold, then the signal has a regular waveform (i.e., strong periodicity). Further, the lag (shift) of the maximum peak (i.e., N in Fig. 5) can be used to calculate the signal cycle by N/f_s. Normally, a respiration waveform of the detected subject is periodic. Therefore, the maximum peak value in its autocorrelation result should be high, and the signal cycle N/f_s is also the respiration cycle of humans. Since the normal human respiration cycle lasts 2–10 s, we limit the range of the lag from $2 \cdot f_s$ to $10 \cdot f_s$, further obtaining the maximum peak value among this range, which is denoted by respiration autocorrelation value hereafter. Thus, given the threshold of the respiration autocorrelation value, we can determine whether a signal waveform is highly periodic and the cycle is within the range of the normal respiration cycle of humans by analyzing the autocorrelation result of signal amplitude or phase waveform, further classifying whether the signal waveform is a respiration detectable waveform.

However, due to existence of the blind spots observed in Sect. 2, we cannot identify all the respiration detectable waveforms using amplitude or phase waveform individually. Therefore, if we can prove the complementarity of respiration detectable portions between signal amplitude and phase waveforms, then we can utilize the complementarity to identify a respiration detectable waveform. We first show that amplitude and phase are complementary to each other theoretically.

The received radar signal $\boldsymbol{H}$ is the superposition of all the path components in the same distance bin as human, and can be divided into two components: the static component $\boldsymbol{H_s}$ and the dynamic component $\boldsymbol{H_d}$. $\boldsymbol{H_s}$ consists of reflection paths from different stationary body parts (e.g., head and legs) and static objects in the same distance as human in the environment, while $\boldsymbol{H_d}$ is mainly determined by the reflection path from dynamic body part (i.e., chest while breathing). $\boldsymbol{H}$ rotates synchronously with $\boldsymbol{H_d}$. Supposing that $\boldsymbol{H_d}$ rotates 360° clockwise from point A in Fig. 6(a), the corresponding amplitude and phase waveforms are plotted in Fig. 6(b).

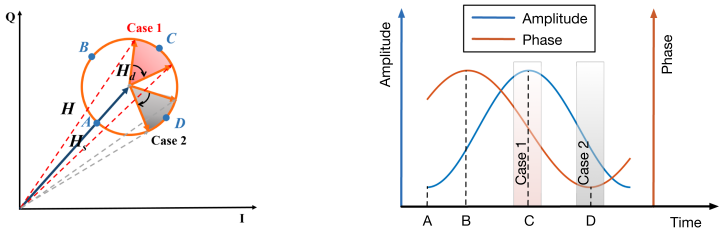

(a) Two arc cases of signals in IQ domain.

(b) Amplitude and phase waveform fragments in two cases.

Fig. 6. Complementarity between amplitude and phase.

However, $\boldsymbol{H_d}$ does not rotate 360° as human breathes (e.g., Fig. 2), but move back and forth along a circular arc. Different arcs in Fig. 6(a) result in different fragments of amplitude and phase waveforms in Fig. 6(b) (e.g., Case 1 and Case 2 in Fig. 6). We find that a bad position for amplitude waveform turns out to be a good position for phase waveform, and vice versa. However, are there any positions where both amplitude and phase change slightly and non-monotonically (i.e., both in bad location) during normal respiration? Some research for Wi-Fi signals [17,22] find that human's normal respiration tends to cause $\boldsymbol{H_d}$ to rotate about 60°. In Fig. 6(b), a window corresponding to 60° cannot find a situation in which both amplitude and phase change slightly and non-monotonically, no matter how much the window slides. Thus we prove the complementarity between amplitude and phase.

Further, we propose that if the respiration autocorrelation value of either amplitude waveform or phase waveform of the signal in current window exceeds the threshold, the signal waveform will be identified as a respiration detectable waveform, and the one with higher respiration autocorrelation value between amplitude and phase waveform will be used to measure respiration rate. If neither of them exceeds the threshold, it reveals that the waveform in current window has poor regularity, and we classify such waveform as other waveform. Figure 7 presents three examples of signal waveforms, where respiration autocorrelation value exceeding threshold is in green, and value not exceeding threshold is in red.

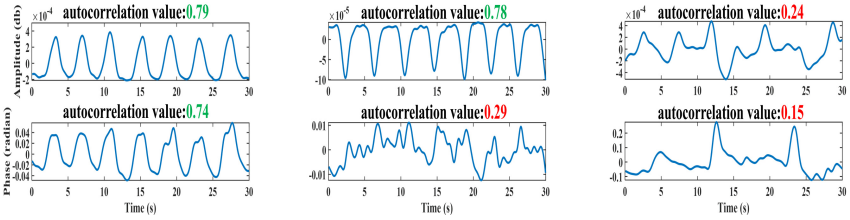

(a) Both amplitude and phase are over the threshold (respiration detectable).

(b) Either amplitude or phase is over the threshold (respiration detectable).

(c) Neither amplitude nor phase is over the threshold (respiration undetectable).

Fig. 7. Signal waveform examples of different respiration autocorrelation values. (Color figure online)

3.3 Estimating Respiration Depth

For the respiration depth distortion (i.e., phase distortion) problem observed in Sect. 2, we analyze it here by projecting the signal onto the complex plane (i.e., IQ domain). As shown in Fig. 8, the decomposition of the signal can be expressed as $\boldsymbol{H} = \boldsymbol{H_s} + \boldsymbol{H_d}$. When the detected subject breathes, $\boldsymbol{H_d}$ rotates along a circular arc, resulting in rotating of $\boldsymbol{H}$ synchronously. Using the phase change $\Delta\Phi$ (i.e., θ_i in Fig. 8) during rotating of received signal $\boldsymbol{H}$, the respiration depth can be estimated by $\Delta d = -\frac{\lambda}{4\pi}\Delta\Phi$. However, the phase change $\Delta\Phi$ is not the real phase change caused by the subject (i.e., θ_c in Fig. 8) due to the effect of $\boldsymbol{H_s}$. Therefore, we need to restore the phase change from θ_i to θ_c so as to estimate the real respiration depth.

In this subsection, we propose a circle fitting based phase restoration algorithm to estimate real human respiration depth during sleep. As described above, the respiration depth distortion problem we observe originates from the phase change distortion. Therefore, we fit a circle based on the signal samples in IQ domain. Then the static component $\boldsymbol{H_s}$ can be eliminated by translating the circle center to the origin of coordinates [7]. As a result, $\boldsymbol{H} = \boldsymbol{H_d}$, $\theta_i = \theta_c$ and the phase change is proportional to the displacement of humans. Details are as follows.

Let $X = \{x_i\}_N, x_i \in R^2$ denote the signal samples in IQ domain, $c \in R^2$ denote the fitted circle center, and r denote the radius of the fitted circle. We formalize the following optimization problem to solve c^* and r^*:

$$c^*, r^* = \arg\min_{c,r} \sum_{x_i \in X} (\|\mathrm{x_i} - \mathrm{c}\| - r)^2 \tag{1}$$

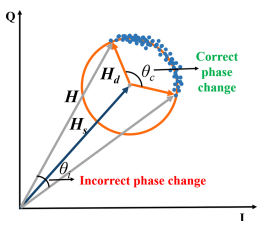

Fig. 8. Signal decomposition in IQ domain.

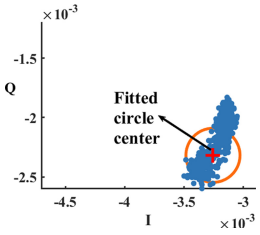

Fig. 9. Example of simple circle fitting result.

It is a nonlinear least squares optimization problem which can be solved using the least squares method in [6]. However, this simple circle fitting method fails to obtain the correct circle when signal samples distribute dispersedly or have low signal quality (such as low signal-to-noise ratio (SNR)), as shown in Fig. 9. Therefore, rather than using all signal samples, we select part of signal samples which can form a regular circular arc as representative samples, and fit a circle based on these samples. The entire algorithm procedure is as follows.

- Firstly, for each respiration detectable waveform, we choose the one with higher respiration autocorrelation value from its amplitude and phase waveform as the final respiration waveform.
- Secondly, we find all peaks and valleys of the final respiration waveform. To remove the fake peaks and valleys, we add two constraints to the peak/valley identification. (i) We set the minimum distance between two neighboring peaks or valleys to $60 \cdot f_s/br_{max}$, where f_s is the radar sampling frequency and br_{max} is human's maximum possible respiration rate (30 bpm in this paper). (ii) We compare each peak or valley to the samples within a window of length $60/br_{max}$ centered at itself. The peak or valley should be the maximum or minimum one within the specified window. Otherwise, it is identified as a fake peak or valley and removed.
- Thirdly, we treat all neighboring peak-to-valley and valley-to-peak waveforms as candidate waveforms. Then, we fit the circle using the least squares method, based on the signal samples selected from all samples by the index range of each candidate waveform. Supposing that there are K candidate waveforms in a 30 s window, we get K candidate circle centers c_j and K candidate radii r_j at last, where $j \in [1, K]$. We calculate the fitting error e_j for each candidate:

$$e_j = \frac{1}{N} \sum_{i=1}^{N} (\|x_i - c_j\| - r_j)^2, j \in [1, K] \tag{2}$$

- Lastly, we choose the circle center with the lowest fitting error as the final circle center, as shown in Fig. 10. We can see that our method solves the problem in Fig. 9.

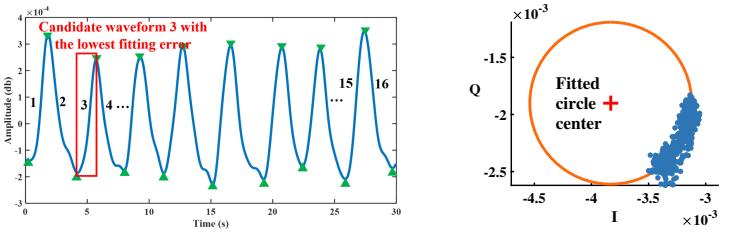

(a) All candidate waveforms of a 30s window in time domain.

(b) Circle fitting result.

Fig. 10. Example of circle fitting result using our method.

After obtaining the final circle center, we eliminate the static component $\boldsymbol{H_s}$ from the signal and calculate its phase waveform. Then, we locate all peaks and valleys within current 30 s window, and obtain phase changes between all pairs of neighboring peak and valley. Finally, the respiration depths are estimated by $\Delta d = -\frac{\lambda}{4\pi}\Delta\Phi$.

3.4 Capturing Respiration Patterns

Table 1 shows four respiration patterns which are clinically significant. If these respiration patterns are detected to occur frequently during sleep, then the detected subject may suffer from the corresponding respiration-related disease.

From Table 1, we can see that Tachypnea pattern and Kussmaul pattern can be identified by setting thresholds on respiration rate and respiration depth, respectively. Rapid change pattern of respiration rate can be identified by setting the threshold on the respiration rate. We adopt a 30 s sliding window with 1 s sliding step to recognize these three respiration patterns from the respiration detectable waveforms.

The apnea pattern is identified from the other waveforms. We use a 10 s sliding window with 1 s sliding step to scan the waveforms, and calculate the variance of the waveform in each window. If the variance of the current window drops by α percent compared to the previous normal window, and is less than a pre-defined threshold β (α, β are set to 0.8 and 8.3×10^{-5}, respectively), we consider apnea occurs in the current window, where β is used to avoid our algorithm identifying the respiration depth change as apnea. By recording the starting time of the first apnea window and the ending time of the last apnea window, we can obtain the duration of the apnea pattern.

Table 1. Four respiration patterns.

Respiration pattern	Definition	Clinical significance
Apnea	Breathing stops for at least 10 s	Frequent apnea relates to SAS
Tachypnea	Breathing is fast but shallow with respiration rate over 24 bpm	Seen in respiratory muscle paralysis, severe bullae and pulmonary diseases such as pneumonia, pleurisy and pneumothorax
Kussmaul	Breathing is slow but deep	Seen in severe metabolic acidosis, such as diabetic ketoacidosis and uremic acidosis
Rapid change of respiration rate	Respiration rate rapidly change from fast to slow or from slow to fast	Slowed respiration is commonly associated with shock and apparent intracranial pressure increase. Increased respiration is commonly associated with fever, anemia, hyperthyroidism, pneumonia and pleurisy

4 Evaluation

4.1 Experimental Setup

Prototype Implementation. We employ a COTS IR-UWB radar XETHRU model X4M05 to collect signals. The radar has the center frequency of 7.3 GHz, the bandwidth of 1.4 GHz, and the sampling frequency of 23.328 GHz. Considering the effect of human's respiration frequency and SNR, we set the frame per second to 17. The radar is connected to a Raspberry Pi via a Dupont line, and all of them are packaged as a compact device, whose appearance and internal structure are shown in Fig. 11. We implement the prototype in Matlab. The demo video is provided at https://youtu.be/lEmYbo8kydA.

Data Collection. Our experimental scenario is shown in Fig. 12. Our device is placed at the bedside of the bedroom and orientates towards the sleeper. We recruit 7 volunteers aged from 22 to 34 years old and collect the data of 17 nights (108 h in total).[1]

Ground Truth. We adopt a 3-lead sleep monitor i.e., Heal Force PC-3000 as shown in Fig. 12, to record respiration rates which are treated as the ground truth. A high-definition camera (i.e., an ONTOP FHD camera) is employed to record real-time waveforms displayed on the sleep monitor. Meanwhile, we use an infrared camera (i.e., EZVIZ C6CN camera) to record the sleep scenes overnight, which is used as the ground truth of human movements.

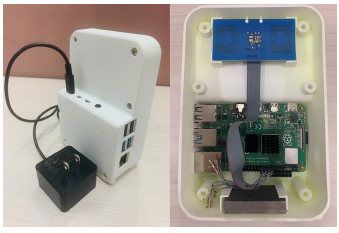

Fig. 11. Appearance and internal structure of our device.

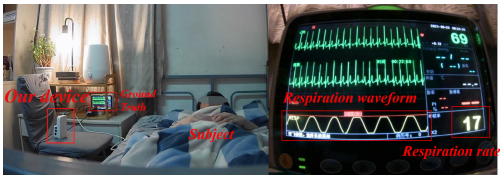

Fig. 12. Experimental setting and ground truth device.

4.2 Overnight Respiration Detection Performance

Respiration Rate Estimation Evaluation. The estimation error of respiration rate is defined as the absolute value of the difference between the estimated respiration rate R_E and the ground truth R_G, i.e., $|R_E - R_G|$. For evaluating the

[1] The data collection procedure was approved by the Institutional Review Board (IRB). Each volunteer is required to sign an informed consent form before the experiments.

estimation errors of our system, two algorithms presented by Raheel et al. [13] and Liu et al. [9] respectively are chosen as competitors. Here, Raheel et al. employ a UWB radar to estimate human respiration rates and heart rates when humans are still. Liu et al. employ a Wi-Fi device to monitor vital signs during overnight sleep. We implement their algorithms and migrate them to our UWB radar. Using our sleep data as input, we execute all three algorithms and get the experimental results as shown in Fig. 13 and Fig. 14.

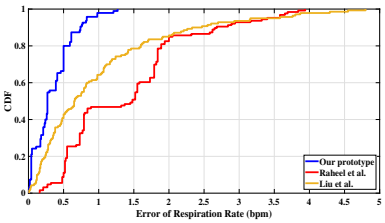

Fig. 13. CDFs of respiration rate estimation errors.

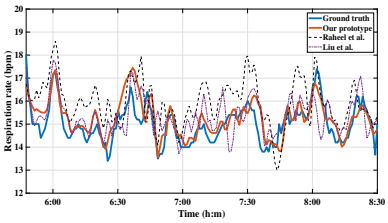

Fig. 14. Respiration rate curves of a certain interval of one night.

Firstly, as a case study, Fig. 14 shows the respiration rate curves of the same subject within the same interval under different algorithms, which shows that our curve fits the ground truth curve best. Secondly, Fig. 13 shows the cumulative distribution functions (CDFs) of the respiration rate estimation errors of three algorithms. We can see that our system achieves a median error of 0.27 bpm and a maximum error of 1.27 bpm, while the median and maximum error of Raheel et al. are 1.27 bpm and 3.94 bpm, respectively, and the median and maximum error of Liu et al. are 0.66 bpm and 4.80 bpm, respectively. In brief, our system achieves the lowest respiration rate estimation errors.

Respiration Detection Rate Evaluation. The respiration detection rate is defined as the ratio of the duration where respiration is detectable over the duration of the entire night's sleep. We derive two variants from our algorithm, one using amplitude alone and another using phase alone. Figure 15 and Fig. 16 show the average respiration detection rates and respiration rate estimation errors of three algorithms. We can see that our algorithm achieves a respiration detection rate of 82.99% and a median estimation error of respiration rate of 0.27 bpm. As a comparison, the respiration detection rate and median respiration rate estimation error are 78.43% and 0.34 bpm for the amplitude variant and 78.05% and 0.27 bpm for the phase variant, respectively. Experimental results demonstrate that our algorithm not only finds more respiration detectable waveforms, but also reduces the estimation error of respiration rate.

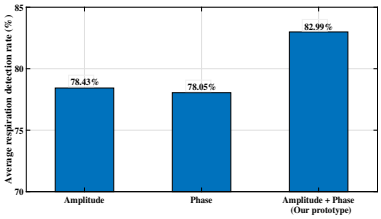

Fig. 15. Respiration detection rate.

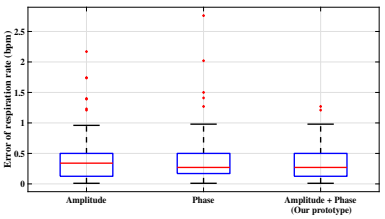

Fig. 16. Respiration rate estimation error.

4.3 Fine-Grained Respiration Detection Performance

Respiration Depth Detection Evaluation. We evaluate the respiration depth restoration performance of the proposed circle fitting based algorithm under different respiration depths and positions by the following experiments. Firstly, the subjects with chest facing the radar are asked to perform normal respiration for 30 s, then deep respiration for 30 s and then gradually return to

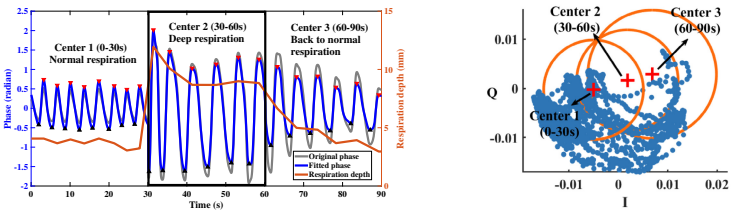

(a) Respiration depth estimation under varying respiration depths.

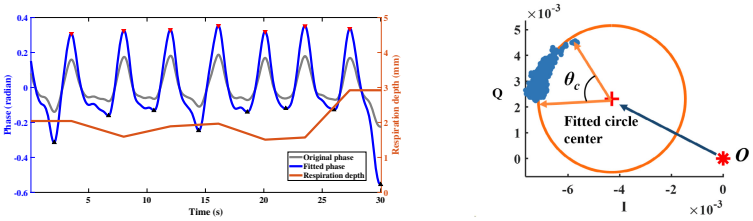

(b) Respiration depth estimation under good position of phase.

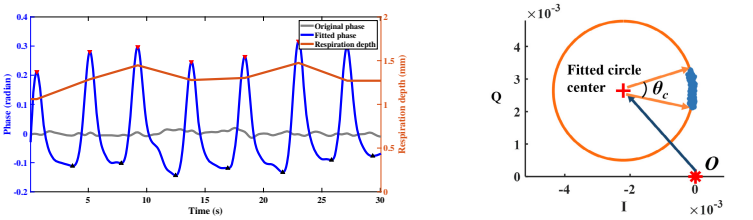

(c) Respiration depth estimation under bad position of phase (blind spot).

Fig. 17. Respiration depth evaluation.

normal respiration in the last 30 s. By this way, we simulate a respiration pattern whose phase varies largely over time. The experimental results are shown in Fig. 17(a), where our algorithm fits a new circle center every 30 s, and is able to restore more realistic change in respiration depth. Secondly, the subjects are required to adjust the orientation of their chests towards the radar so that the phase waveforms generated by their reflections are regular (subjects in a good position for phase to detect respiration) or disordered (subjects in a bad position for phase to detect respiration). The experimental results demonstrate that our algorithm can successfully restore the respiration depth regardless of whether the subjects are in a good position (Fig. 17(b)) or a bad position (Fig. 17(c)) for phase to detect respiration.

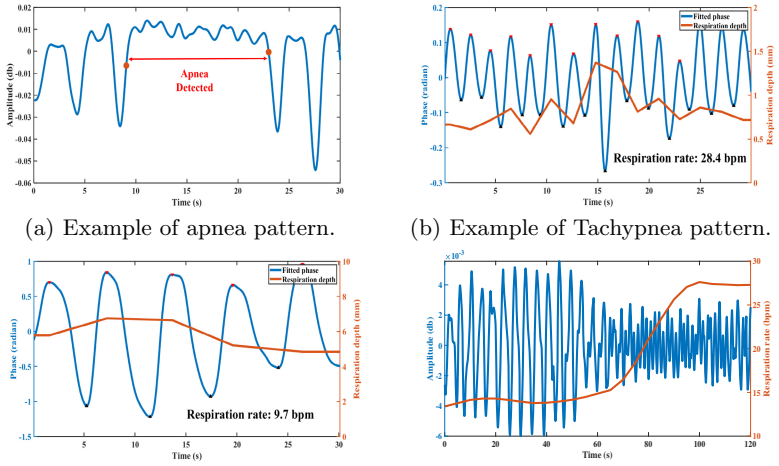

(a) Example of apnea pattern.

(b) Example of Tachypnea pattern.

(c) Example of Kussmaul pattern.

(d) Example of rapid change pattern of respiration rate.

Fig. 18. Different respiration patterns.

Respiration Pattern Detection Evaluation. We detect four respiration patterns, including apnea pattern, Tachypnea pattern, Kussmaul pattern and rapid change pattern of respiration rate, from overnight sleep signals.

- **Apnea pattern.** We perform the apnea detection on the sleep data of 17 nights, and find apnea appears five times. We compare them with the respiration waveforms provided by the sleep monitor, and the results show that our algorithm achieves 100% detection accuracy in detecting apnea during sleep. Figure 18(a) shows an example of apnea waveform at a certain night. It can be seen that the respiration waveform between 9 and 23 s becomes flat, and the whole apnea duration lasts for 14 s.

- **Tachypnea pattern and Kussmaul pattern.** Since our overnight data do not contain these patterns, we require the subjects to lie in bed with chest facing the device, and then simulate the patterns for 30 s, respectively. The experimental results show that our algorithm is able to detect these simulated respiration patterns, as shown in Figs. 18(b) and Fig. 18(c).
- **Rapid change pattern of respiration rate.** Since the rapid change pattern of respiration rate did not occur in our overnight sleep data, we require the subjects to perform normal respiration for 60 s, and then rapid respiration for 60 s. The experimental results show that our algorithm is able to detect this simulated respiration pattern, as shown in Fig. 18(d).

5 Related Work

With the development of wireless sensing technology, a number of wireless signal based solutions on vital sign and sleep monitoring have been proposed. Some solutions [12,16] exploit FMCW acoustic signals, and some solutions [2,8,22] exploit Wi-Fi signals. However, acoustic and Wi-Fi signals are sensitive to interference from the environment, thus leading to unstable sensing performance. On the other hand, although the quality of RFID signals is relatively stable, RFID-based solutions have to face the high deployment costs, which causes the difficulty in large scale deployment.

Compared with acoustic, RFID and Wi-Fi signals, radar signals are highly resistant to interference and have strong penetration capability, which make it popular with applications such as ranging, tracking and imaging. Some work has employed radars for vital sign sensing. For example, DoppleSleep [14] employs a commercial 24 GHz short-range Doppler continuous wave radar to continuously track human vital signs, enabling real-time and efficient sleep monitoring. Vital-Radio [3] exploits a FMCW radar to monitor respiration and heart rates, which also supports through-wall and multi-subject sensing. mmVital [20] uses a millimeter wave radar to monitor vital signs. It enables indoor multi-person detection and through-wall detection by introducing directional beamforming methods on the received signal strength information of the 60 GHz millimeter wave. In particular, Raheel et al. [13] use an IR-UWB radar to monitor human respiration and heart rates. Zheng et al. [24] also use an IR-UWB radar to perform in-vehicle vital sign monitoring.

We find existing solutions on respiration and sleep monitoring mainly focus on normal conditions (e.g., subject in a sober state sits in chair or lies in bed), which is not applicable to the overnight sleep scenario. By contrast, our work provides overnight respiration monitoring and can capture four respiration patterns such as apnea, which operates well in real sleep scenarios.

6 Conclusion

In this paper, we implement a prototype which is capable of overnight and fine-grained respiration monitoring. By exploiting IR-UWB radar as the front-end

for data collection, our prototype is contact-free, of high-precision, and easy to deploy. Moreover, our prototype can provide both high detection rates and low estimation errors of respiration rates. Furthermore, it can also recognize four respiration patterns.

In the near future, real clinical experiments are expected to be conducted to evaluate the performance on patient's respiration monitoring. Further, we will extend our work to overnight heartbeat monitoring and sleep stage classification.

Acknowledgments. This work was supported by the National Natural Science Foundation of China under Grants No. 61802373 and No. 62072450.

References

1. Flow chest straps (2018). https://www.wareable.com/wearable-tech/sweetzpot-flow-breathing-chest-strap-2018
2. Abdelnasser, H., Harras, K.A., Youssef, M.: UbiBreathe: a ubiquitous non-invasive WiFi-based breathing estimator. In: Proceedings of the 16th ACM International Symposium on Mobile Ad Hoc Networking and Computing, pp. 277–286 (2015)
3. Adib, F., Mao, H., Kabelac, Z., Katabi, D., Miller, R.C.: Smart homes that monitor breathing and heart rate. In: Proceedings of the 33rd Annual ACM Conference on Human Factors in Computing Systems, pp. 837–846 (2015)
4. Anderson, J.A., Vann, W.F.: Respiratory monitoring during pediatric sedation: pulse oximetry and capnography. Pediatr. Dent. **10**(2), 94–101 (1988)
5. Azagra-Calero, E., Espinar-Escalona, E., Barrera-Mora, J.M., Llamas-Carreras, J.M., Solano-Reina, E.: Obstructive sleep apnea syndrome (OSAS). Review of the literature. Medicina Oral, Patologia Oral y Cirugia Bucal **17**(6), e925 (2012)
6. Chernov, N., Lesort, C.: Least squares fitting of circles. J. Math. Imaging Vis. **23**(3), 239–252 (2005)
7. Jiang, C., Guo, J., He, Y., Jin, M., Li, S., Liu, Y.: mmVib: micrometer-level vibration measurement with mmwave radar. In: Proceedings of the 26th Annual International Conference on Mobile Computing and Networking, pp. 1–13 (2020)
8. Khamis, A., Kusy, B., Chou, C.T., Hu, W.: WiRelax: towards real-time respiratory biofeedback during meditation using WiFi. Ad Hoc Netw. **107**, 102226 (2020)
9. Liu, J., Chen, Y., Wang, Y., Chen, X., Cheng, J., Yang, J.: Monitoring vital signs and postures during sleep using WiFi signals. IEEE Internet Things J. **5**(3), 2071–2084 (2018)
10. Luo, J., Ying, K., Bai, J.: Savitzky-Golay smoothing and differentiation filter for even number data. Signal Process. **85**(7), 1429–1434 (2005)
11. Młyńczak, M., Cybulski, G.: Improvement of body posture changes detection during ambulatory respiratory measurements using impedance pneumography signals. In: Kyriacou, E., Christofides, S., Pattichis, C.S. (eds.) XIV Mediterranean Conference on Medical and Biological Engineering and Computing 2016. IP, vol. 57, pp. 167–171. Springer, Cham (2016). https://doi.org/10.1007/978-3-319-32703-7_34
12. Nandakumar, R., Gollakota, S., Watson, N.: Contactless sleep apnea detection on smartphones. In: Proceedings of the 13th Annual International Conference on Mobile Systems, Applications, and Services, pp. 45–57 (2015)
13. Raheel, M.S., et al.: Breathing and heartrate monitoring system using IR-UWB radar. In: 2019 13th International Conference on Signal Processing and Communication Systems (ICSPCS), pp. 1–5. IEEE (2019)

14. Rahman, T., et al.: DoppleSleep: a contactless unobtrusive sleep sensing system using short-range doppler radar. In: Proceedings of the 2015 ACM International Joint Conference on Pervasive and Ubiquitous Computing, pp. 39–50 (2015)
15. Vorona, R.D., Winn, M.P., Babineau, T.W., Eng, B.P., Feldman, H.R., Ware, J.C.: Overweight and obese patients in a primary care population report less sleep than patients with a normal body mass index. Arch. Intern. Med. **165**(1), 25–30 (2005)
16. Wang, A., Sunshine, J.E., Gollakota, S.: Contactless infant monitoring using white noise. In: The 25th Annual International Conference on Mobile Computing and Networking, pp. 1–16 (2019)
17. Wang, H., et al.: Human respiration detection with commodity WiFi devices: do user location and body orientation matter? In: Proceedings of the 2016 ACM International Joint Conference on Pervasive and Ubiquitous Computing, pp. 25–36 (2016)
18. Wang, T., Zhang, D., Zheng, Y., Gu, T., Zhou, X., Dorizzi, B.: C-FMCW based contactless respiration detection using acoustic signal. In: Proceedings of the ACM on Interactive, Mobile, Wearable and Ubiquitous Technologies, vol. 1, no. 4, pp. 1–20 (2018)
19. Wang, Y., Zheng, Y.: TagBreathe: monitor breathing with commodity RFID systems. IEEE Trans. Mob. Comput. **19**(4), 969–981 (2019)
20. Yang, Z., Pathak, P.H., Zeng, Y., Liran, X., Mohapatra, P.: Monitoring vital signs using millimeter wave. In: Proceedings of the 17th ACM International Symposium on Mobile Ad Hoc Networking and Computing, pp. 211–220 (2016)
21. Yim, D.H., Cho, S.H.: An equidistance multi-human detection algorithm based on noise level using mono-static IR-UWB radar system. In: Future Communication, Information and Computer Science: Proceedings of the 2014 International Conference on Future Communication, Information and Computer Science (FCICS 2014), Beijing, China, 22–23 May 2014, p. 131. CRC Press (2015)
22. Zeng, Y., Wu, D., Gao, R., Gu, T., Zhang, D.: FullBreathe: full human respiration detection exploiting complementarity of CSI phase and amplitude of WiFi signals. In: Proceedings of the ACM on Interactive, Mobile, Wearable and Ubiquitous Technologies, vol. 2, no. 3, pp. 1–19 (2018)
23. Zeng, Y., Wu, D., Xiong, J., Yi, E., Gao, R., Zhang, D.: FarSense: pushing the range limit of WiFi-based respiration sensing with CSI ratio of two antennas. In: Proceedings of the ACM on Interactive, Mobile, Wearable and Ubiquitous Technologies, vol. 3, no. 3, pp. 1–26 (2019)
24. Zheng, T., Chen, Z., Cai, C., Luo, J., Zhang, X.: V2iFi: in-vehicle vital sign monitoring via compact RF sensing. In: Proceedings of the ACM on Interactive, Mobile, Wearable and Ubiquitous Technologies, vol. 4, no. 2, pp. 1–27 (2020)